
OLB: AN OPEN LORA BUOY FOR COASTAL WATER MEASUREMENTS

PREPRINT

Lars Willas Dreyer^{1,*}, Andrea Pferscher², Riccardo Sieve²,
Jean Rabault³, Atle Jensen¹, Einar Broch Johnsen², and Gaute Hope⁴

¹Department of Mathematics, University of Oslo, Norway, larswd@proton.me, atlej@math.uio.no

²Department of Informatics, University of Oslo, Norway, {andreas, riccasi, einarj}@ifi.uio.no

³IT Department, Norwegian Meteorological Institute, Norway, jean.rblt@proton.me

⁴R&D Department, Norwegian Meteorological Institute, Norway, gauteh@met.no

January 28, 2026

ABSTRACT

Oceanographic instrumentation technology is currently under rapid transition towards increasingly open-source technology. Open-source buoys compete with commercial and closed-source buoys both in price, functionality and availability. Long-range radio (LoRa) is a communication technology which is inexpensive both in terms of data transfer cost and power without the need for pre-existing infrastructure. In this paper, we present OLB, an open-source drifter buoy using LoRa for coastal water measurements. OLB is designed to be reliable, low-cost, modifiable and power efficient. We present validation experiments demonstrating that OLB can achieve a radio telemetry range of more than 2 kilometres, and has an expected battery lifetime of up to seven months. Finally, we discuss the role and contribution of OLB in the space of open-source instrumentation and ocean modelling.

1 Introduction

One of the most important mechanisms regulating oceanic dynamics and ocean health is ocean circulation. These dynamics are active from the global scale, such as the Gulf-stream [Palter, 2015], to the local scale, such as fish egg transport [Sundby and Kristiansen, 2015, Norcross and Shaw, 1984, Romagnoni et al., 2020], pollutant transport such as oil spill drift [Le Hénaff et al., 2012], and coastal nitrate deposition [Sugimoto et al., 2009, Sigleó et al., 2005]. Coastal environments are especially vulnerable to human activity [Roukounis and Tsihrintzis, 2022]. Increased precipitation due to climate change might result in increased river erosion [Toimil et al., 2017], and the same rivers also constitute one of the main pathways for industrial and agricultural pollution by humans [Vikas and Dwarakish, 2015, Howarth et al., 2000]. High-quality measurements of oceanographic flow are essential to understand ocean dynamics and ocean health.

Measuring the ocean has historically been a challenging task, as researchers had to perform measurements manually and often *in-situ* (e.g., [Zielinski, 2021]). Satellite imaging has drastically increased our ability to measure and model the ocean since the first satellite was launched in 1977 [Freeman et al., 2010]. Today, we can get daily measurements of the global sea surface at the kilometre scale [Amani et al., 2022]. However, this resolution alone is often insufficient to capture important information about flow, especially in scenarios where the important length scales are smaller than those of the open deep sea.

An alternative to in-person measurements is sensor buoys, which allow us to measure the system of interest *in-situ*. Such instruments have been commercially available since the 1960s [Datawell BV, 2006, Datawell BV]. These instruments

* Corresponding author.

have historically been priced in the range of 10-100 thousand USD [Rabault et al., 2020], and been closed-source hardware with limited customizability. The price of a sensor buoy fell in the early 2000s with increased competition from other commercial buoys [Raghukumar et al., 2019] and closed-source academic buoys [da Silva et al., 2022, Kohout et al., 2015, Wilkinson et al., 2007]. The availability and reduced price of these buoys made it much more feasible to collect larger amounts of data of the ocean and measure ocean conditions for which in-person measurements are too difficult or dangerous to perform.

Several prognostic models of ocean flow have been developed to understand phenomena such as oil spills [Periáñez, 2020, Korotenko et al., 2010], the dispersion of brine from desalination [Pereira et al., 2021, Wood et al., 2020], and the transport of submerged bodies (such as humans at sea) [Hackett et al., 2006, Tu et al., 2021]. However, these ocean models still suffer from a lack of data, either in sufficient resolution or in its entirety [Fringer et al., 2019, Cavalieri et al., 2025]. In a recent workshop in Oslo in March 2025, the need for an increased amount of sensor data for forecasting in general, and the arctic in particular, was an ongoing topic of discussion amongst representatives from many of the meteorological agencies across Europe and North America [Müller, 2025].

Recently, several low-cost open-source instruments have been released. These make the process of taking oceanographic measurements easier, less expensive, and more customizable. Notable examples include the *Small Friendly Buoy* (SFY) [Hope et al., 2025] to measure waves close to the coast, the *OpenMetBuoy* (OMB) [Rabault et al., 2022] to measure wave activity under arctic and open ocean conditions, and the *microSWIFT* buoy [Thomson et al., 2024] which is capable of measuring wave activity, temperature, and salinity and is deployable from an aircraft. These sensor buoys are part of a recent trend: a shift from commercial, closed-source, and expensive buoys toward cheaper, open-source, and scientist-developed instrumentation. The open-source aspect in particular is an important development, because openly available source code serves the dual purpose of both allowing the users to tailor the instrument to their specific use case and simultaneously opening up the entire software implementation to external scrutiny. This transparency allows any user to check that the framework works as stated, while reducing the chance for undiscovered error in the firmware to persist indefinitely.

Most of these buoy designs utilize a GSM or an Iridium satellite communication solution to transmit buoy measurement to the end user. Iridium uses satellite communication [Maine et al., 1995] and therefore offers a reliable connection even in distant or inhospitable environments such as the Arctic [Rabault et al., 2022], while GSM uses the cell phone network to transmit possibly large amounts of data quickly [Hope et al., 2025]. However, both solutions consume large amounts of power (communication is the main power sink for both the OMB and the SFY buoys) and may come with significant cost in data transfer fees (in particular when using Iridium). One way to circumvent these limitations is to use low-power communication protocols such as LoRa [Devalal and Karthikeyan, 2018]. LoRa is a free band radio technology that transmits radio signals at a sub-GHz frequency with low power consumption, over a range of up to a few kilometres. Compared to GSM and Iridium, LoRa is more limited in range, but offers a cheap and power-efficient mode of data transfer in regions or applications where the distance to a receiving node can (to a certain extent) be controlled. Several remote sensor projects have used LoRa as their communication protocol. The drifter buoy of Majumder et al. [2024] uses LoRa together with an *Internet of Things*-network, while Raphael et al. [2025] use a network of LoRa devices surrounding a central base station with a satellite communication setup. However, neither of these buoy designs is open source, making both buoys difficult to adapt according to specific needs.

The paper presents OLB, a new open-source LoRa-based drifter buoy and base station framework made for measuring circulation and coastal currents. This buoy framework offers a simple, reliable and inexpensive way to measure coastal flow and ocean dynamics, with a battery lifetime of several months. Both the default code and hardware configurations are publicly available on GitHub, and come with a modular setup which can readily be extended to include additional functionality. Furthermore, the OLB buoys are relatively small and light, allowing field experiments to be performed without the need for more specialized transportation than a regular car, as well as ensuring that the base station installation is largely nonintrusive. We report on validation data from both radio range experiments and a full-system reliability experiment, demonstrating a battery lifetime of more than three months.

We expect that the open-source implementation of the OLB will allow researchers to conduct experiments to validate numerical and theoretical models at a significantly reduced cost without sacrificing the amount of collected data. A large deployment of buoys will, for example, yield a data ensemble of the oceanographic flows in coastal environments at a fraction of the cost of commercial alternatives. These data ensembles can be used to validate numerical models, feed information to digital twins, and other actors interested in coastal climates, all with high spatial and time resolution in the area of interest. Furthermore, by providing an *adaptive measurement period*, the OLB is able to sample areas of high activity with higher temporal resolution, such as rivers, estuaries, and local currents.

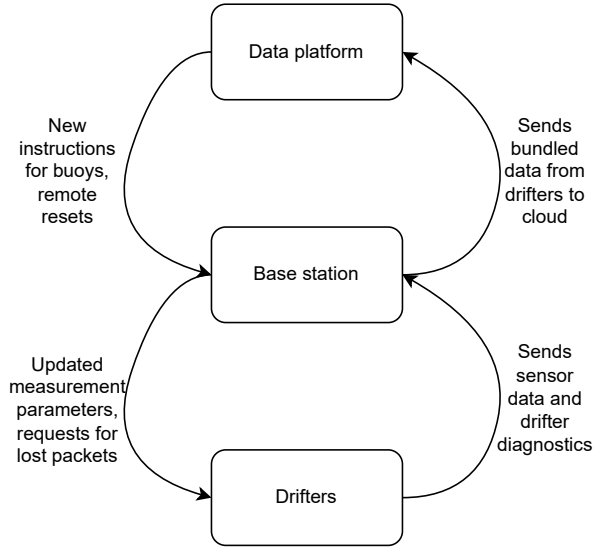


Figure 1: Relationship diagram showing how the different parts of the OLB framework interact. Drifters are deployed in a coastal area within range of one or more base stations. They gather in situ measurements, which are sent via LoRa to a base station, which then bundles the data and sends them to the backend data platform over GSM. Conversely, the data pipeline allows the user to remotely give instructions to both the base stations and the drifters by sending instructions from the backend data platform to the base stations, and from there to the buoys.

2 OLB: An Open LoRa Buoy Framework

OLB is both a buoy and a framework for monitoring coastal water environments. The framework consists of a drifter buoy design, a base station design, and a visualization/data platform design. The relationship between the different parts of the framework is visualized in Figure 1.

In our default configuration, the drifters are surface drifters equipped with a GPS, one or more thermometers, an SD card, and a LoRa transceiver. In addition, more sensors can be attached by the user through a variety of interfaces (I2C, SPI, serial, analogue). The LoRa transceiver also acts as the main control unit of the drifter. The default drifter firmware is customizable through a configuration file, with important parameters explained in Tables 1 and 2 (these are detailed in the following sections). Hence, the OLB drifter is quite configurable even for a user with limited programming knowledge, and it is adaptable to the needs of the end user. In the GitHub repository, example codes show how it is possible to use each component of the drifter separately, in case a user would prefer to write their own firmware from scratch. The base firmware workflow of the buoy consists roughly of two phases after the initial setup phase. The first phase is the measuring phase, where the buoy reads each attached sensor a total of n_m times every T_m minutes (as shown in Table 1), before filtering and averaging all the readings into a single mean measurement value for each sensor. In the second phase, the buoy will start looking for a base station to transmit data and to receive for new instructions. This phase occurs after both the time limit T_t between measurements and the minimum measurement threshold N_m have been exceeded. A detailed overview of the included firmware is given in Section 3.4. A diagram of the protocol is shown in Figure 5.

The second component in the OLB framework is the base station, which acts as an intermediary between the user and the buoys, as it transmits data from the buoys to a cloud backend and is additionally equipped with the functionality necessary to remotely push setting updates to the buoy firmware during deployment. The base station is controlled by the same main controller unit and radio transceiver as the drifter, but unlike the drifter, it is not equipped with any sensors. In addition, the base station is equipped with a GSM modem, to allow communication with cloud-based servers. The base station is designed to have a long battery life and to be mounted at a coastal vantage point with GSM coverage, close to the area where the buoys are deployed. Remark that the LoRa radio protocol has reduced range if there is no line of sight between the sender and receiver, so the user must take some care when placing base stations in the field.

Buoy parameter	Default value	Remote update	Notes
Reception frequency f_r	863 MHz	No	Legal bands subject to local jurisdiction
Beacon frequency f_b	868 MHz	No	Legal bands subject to local jurisdiction
Measurement period T_m	15 min	Yes	-
Transmission period T_t	30 min	Yes	Sets an upper bound on the transmission period if measurements per transmission is low
Beacon message period T_b	3 min	No	-
Measurements per transmission N_m	4	Yes	Sets an upper bound on the transmission period if transmission period is low.
Max number of measurements stored in memory, N_{\max}	50	No	-
Readings per measurement n_m	15	No	Higher number of readings for a single measurement yields better filtered estimate
Max GPS read time T_{GPS}	3 min	No	Max time the GPS will spend looking for a fix.
LoRa bandwidth B_L	125 kHz	No	-
LoRa spread factor s_f	8	No	Must be an integer between 5 and 12
LoRa coding rate c_r	6	No	Must be an integer between 5 and 8
LoRa output power W_{LoRa}	20 dBm	No	Must be an integer between -9 and 22
Target distance between measurements d_{target}	200 m	Yes	For the adaptive measurement period described in Equation 1
Velocity threshold v_t	1.0 m/s	Yes	Threshold for the adaptive measurement algorithm to activate.

Table 1: The most important parameters for the OLB buoys, all of which are configurable by the user in the configuration file, their default values, whether they can be changed remotely and important notes about the parameters.

Buoy functionality	Default setting	Notes
Remove outliers	Enabled	Enable/Disable σ -filtering
Enable motion detection	Enabled	Adaptive measurement period as detailed in Equation 1
Perform handshake	Enabled	Toggle handshake portion of Figure 5.
Log every reading	Enabled	Toggle if the OLB should store all readings to SD card, or just filtered mean.
Transmit deployment message	Disabled	Enable to ensure that the buoy will send an initial message to a nearby base station in range before entering the main program loop.

Table 2: The most important flags which can be enabled or disabled by the user to activate or deactivate parts of the OLB functionality.

The third component of the OLB framework is a visualization/data platform. The data platform offers a web page frontend that allows monitoring the deployed buoys, visualizing and inspecting the collected data, and issuing new instructions to the buoys via the deployed base stations. The data platform is, unlike the base stations and buoys, not strictly necessary for the framework to operate, as the GSM module in the base station transmits directly to the online data repository; we here use the notehub.io data platform maintained by Blues, the manufacturer of the base station GSM module. The OLB data platform is a frontend made to provide easier and more intuitive interaction with the buoys during deployment.

3 The Design of the OLB Buoy

The OLB buoy is the data collection component of the OLB framework. It consists of a main controller unit with a radio transceiver, a GPS, an SD card reader/writer and any additional measuring devices installed by the end user. In this section, we detail the software, hardware and functionality of the OLB buoy.

3.1 The Main Controller

The main controller unit's primary job is to gather readings from the attached sensors, post-process these readings and then store them either in RAM or in local storage until the data can be recovered. Furthermore, the main controller should also facilitate the data transfer protocol between the drifter and base station.

The main controller unit of the OLB buoys is the Wio-E5 Mini board by [Seeed Studio \[2023\]](#). The Wio-E5 Mini board was chosen as the main board for the OLB buoys in part due to the price (~ 20 USD) and in part because it incorporates a low-cost high-performance main controller unit that has a built-in LoRa transceiver [[Seeed Studio, 2023](#)]. This transceiver is the sole communication unit of an OLB buoy, and transmits any data to a nearby base station if there are any. In the case where no base station is present within LoRa range, the buoy will try again at a later time (default 15 min). Each Wio-E5 Mini board has a 12 byte unique identifier number, which we use as the identifier of the associated buoy. The LoRa protocol, being very low power, has a limited range, and we have observed ranges of up to 2 km in ocean waters, but ranges of up to 10 km have been observed in more ideal conditions [[Aref and Sikora, 2014](#), [Falanji et al., 2022](#)]. During the setup of a field experiment, we were able to attain a range of up to 5.4 km while the buoy was on land.

The Wio-E5 Mini board uses a low-cost high-performance STM32WL55JC microcontroller unit, with a 32-bit 42 MHz processor, 64 kb RAM and comes with a built-in LoRa module. Furthermore, the STM32WL55JC comes equipped with a wide range of interfaces (several I2C, SPI, serial buses, as well as digital and analogue pins), facilitating an easy way of adding additional sensors and functionality to the buoy, while still leaving a significant amount of embedded memory and compute left for the end user. The firmware uploaded to the Wio-E5 Mini board is programmed using Platformio IDE, and is uploaded to the microcontroller via a ST-LINK debugger, and the firmware is openly available online.¹

3.2 Sensor Components

The OLB buoys are additionally equipped with a thermometer and a GPS. The GPS measurements ensure both a spatial and temporal location for the other sensor readings. In the default software, a faulty GPS will result in a firmware freeze, to minimize the risk of deploying a faulty drifter. The thermometer is a cheap and power efficient instrument which allows the buoy to capture surface temperatures, or temperatures further down the water column. These values are important parameters in many operational models in meteorology, such as GOTM [[Umlauf and Burchard, 2005](#)] or ROMS [[Moore et al., 2011](#)]. An overview of all components of the OLB buoy, their function, and a link to the page where they were ordered, together with prices, is given in Table 3, and the wiring of these is shown in Figure 2.

Each buoy is, in the default configuration, equipped with a single DS18B20 [[Semiconductor, 2025](#)] thermometer, which uses a one-wire protocol to transmit measured temperature data to the main controller unit. The thermometer has an operational range of -10–85 degrees centigrade, with an absolute accuracy out of the box of ± 0.5 degrees centigrade. However, the dynamic accuracy is significantly higher and the repeatability and stability of the sensors allow custom calibration and higher accuracy. Specifically, the thermometers can be calibrated with a three-point calibration, improving the absolute accuracy to approximately 0.1 degrees centigrade (for more information, see [Müller et al. \[2024, 2025\]](#)). Furthermore, the DS18B20 can be daisy-chained to enable measurement of a temperature profile. DS18B20 sensors are calibrated prior to deployment and the calibration is applied as a post-processing step, as the buoy does not store calibration data in memory, meaning an a-posteriori lookup table which matches thermometer to calibration curve is necessary to get the most accurate temperature readings. While post-deployment calibration is possible, we advise against it due to the risk of not recovering the buoy after deployment.

The GPS measurements have a precision of 3 meters, which is a hard limit of the instrument [[Adafruit, 2014](#)]. During a measurement cycle, the GPS is always read first as the GPS fix information is necessary both for spatial localization of measurements and to update the real time clock of the drifter. A single GPS data reading contains a value for latitude, longitude, speed and direction, as well as a (POSIX) timestamp and a reading ID. This ID allows for remote recovery of lost data through instructions transmitted to the buoy from the base station.

The open-source firmware and hardware in the OLB buoy allows for user modifications, both in terms of minor software adjustments, such as changes to the measurement and transmission protocol as well as major additions such as new hardware. The default firmware contains examples of how to add additional sensor firmware. The PCB has a second row of pins for each pin on the OLB. Furthermore, the firmware is designed in a containerized fashion, meaning the radio transceiver and SD card logger is applicable to new hardware. In the GitHub repository, we present an example of how to add a turbidity sensor to the OLB.

¹<https://github.com/larswd/OpenLoraBuoy>

Component	Function	Producer	Price (per 08-2025) [USD]
Wio-E5 Mini	Main controller unit, radio transceiver	Seeed studio	21.90
Adafruit Ultimate GPS	GPS sensor, RTC	Adafruit	29.95*
DS18B20	Thermometer	Sparkfun	10.95
Micro-SD card	SD card writer/reader	Adafruit	7.50
breakout board+			
Pololu 3.3V S7V8F3	Step up/down voltage regulator	Pololu	9.95*
SD card	On buoy data storage	Adafruit	9.95
Saft LSH20	13 Ah Li-battery	Saft	18*
PCB	Base circuit board	JLCPCB	1-6*
Container parts	Waterproof buoy container equipment	-	~15-20
Price per buoy for 5 buoys			126.2
Price per buoy for 50 buoys			115.9

Table 3: The hardware components of the OLB buoy, their function and manufacturer. For convenience, manufacturer names are hyperlinked to the product page where the components were ordered. Prices marked with an asterisk (*) are subject, at the time of writing, to a bulk order discount. In particular, the cost of a PCB is almost exclusively shipping, and the price listed is a price estimate for a single PCB out of an order of 5–30 PCBs. Hence, the final price might be lower than what is listed here for several of the components.

Phase	Current	Phase Duration	Power consumption per day
Inactive mode	0.7 mA	~15 minutes	17 mAh/day
Measuring mode (GPS)	45-60 mA	10-60 seconds ²	40 mAh/day
Measuring mode (Other)	8-10 mA	10 seconds	2 mAh/day
Transmission mode	9-11 mA	1 minute	12.8 mAh/day
Total consumption: bad conditions	-	-	123 mAh/day
Total consumption: moderate conditions	-	-	67 mAh/day
Total consumption: good conditions	-	-	47 mAh/day

Table 4: The power consumption of the OLB buoy during each distinct phase of the firmware execution, the typical duration of each phase, and the amount of power consumed by each phase during a day with moderate conditions. Here, *good conditions* happen when the GPS is quick to get a fix and pulls a low amount of power (average of 50 mA for 10 seconds), *moderate conditions* when the power consumption of the GPS and time is slightly larger (60 mA for 25 seconds), while *bad conditions* occur at the high end of the GPS power use (60 mA for 60 seconds). For the other modes, we assumed a current of 9 mA in the measuring mode (other) phase, and a current of 10 mA in the transmission phase.

3.3 Additional Components

In addition to the sensors, the OLB buoy comes equipped with several supporting components: a battery, a voltage regulator and an SD card writer. The battery used in our tests is a single SAFT LSH20 3.6 V lithium D battery, with a capacity of 13 Ah. The output power is regulated by a 3.3 V step-up/step-down regulator [Pololu Robotics and Electronics, a]. We measured the power usage of the buoy with a multimeter connected in serial between the voltage regulator and the reed switch. Using the currents measured by the sensor (see Table 4), and assuming a full 13 Ah battery, the buoy has an expected lifetime between 3.5 months (worst case) to 9.2 months (best case) of continuous operations, although more rapid measurements and transmissions would decrease the expected lifetime.

The OLB buoy transmits the recorded data and saves it to an SD card via an Adafruit microSD breakout [Adafruit, 2025]. The OLB buoy sleeps for a certain period of time between measurements. The default number of measurements during a given measurement cycle is 10, but this number is configurable in the code. The buoy transmits the filtered (as explained in Section 3.4) average of these 10 measurements as an estimated value for the corresponding measurement cycle. Thereafter, a new mean of all the remaining readings is computed and stored in memory for transmission. However, each individual measurement is saved to the SD card. Hence, if the OLB buoy is recovered, the raw data could be analysed in more detail.

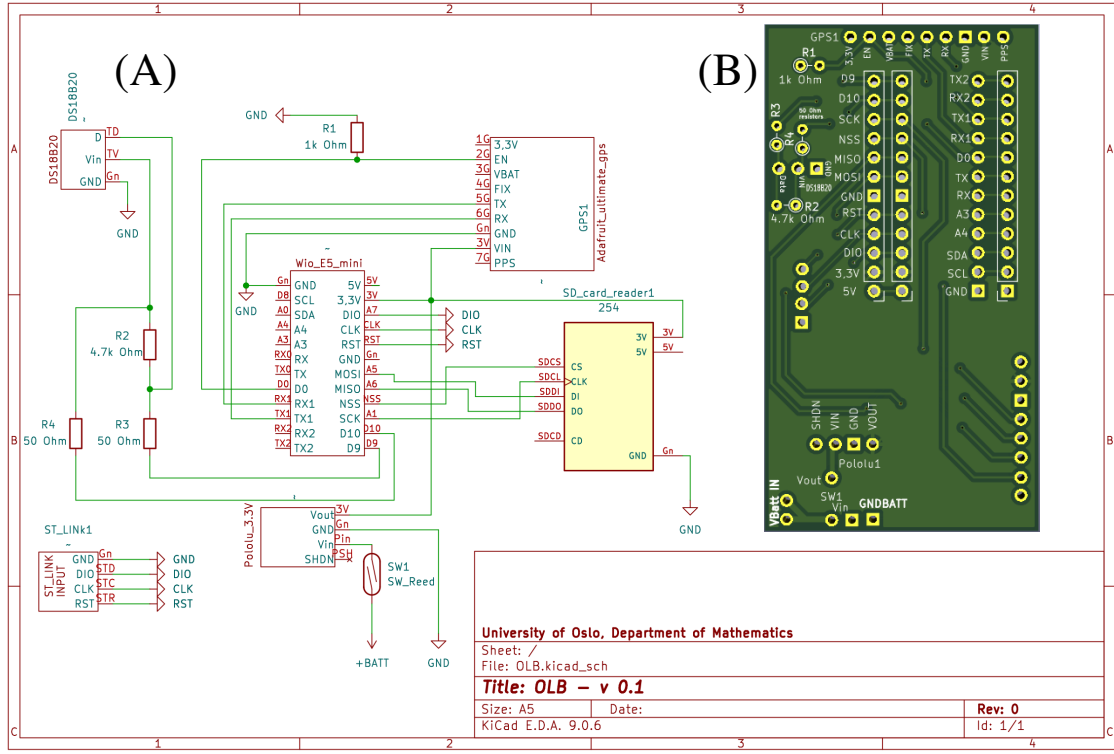


Figure 2: Subfigure (A) shows a schematic for the wiring between each component on the OLB buoy. The reed switch enables the user to turn off the buoy by placing a magnet on a designated spot on the buoy casing. The pull-down resistance between the EN-pin on the GPS and ground is to ensure that the GPS is switched off while not measuring. A small coin cell battery is connected to the GPS to allow it to store fix information even when powered off. Subfigure (B) shows the corresponding printed circuit board (PCB), where the connections depicted in Subfigure (A) are implemented.

3.4 Default Software

OLB is an open-source buoy and hence programmable by the end user to tailor it to a specific use case. It comes with a default software to read, record, and transmit data from all sensors connected to the main controller unit. The default software can be roughly divided into two main stages (*setup* and *measurement and transmission* modes), the latter can be further divided into four stages. The software includes a configuration file in which many parameters relating to buoy functionality, such as measurement frequency, transmission frequency, SD-logging, and motion detection, can be set by the user without the need to alter the software or code any extra functionality. The list of the most important parameters and options present in the configuration file is shown in Tables 1 and 2. Each named variable in this section is listed in these two tables, with the exception of the variables in Equation 1.

The OLB buoy begins in the *setup* mode, in which it first initializes its connections with each connected hardware component, and where it boots up the radio for the first time. Afterwards, the buoy checks that both the radio and GPS are working as intended. If one of these components fails, the buoy will not start logging data. If the transmit deployment message flag is set to true, the buoy will not continue into the main software loop before a connection has been established to a base station. The buoy has a limited capacity for storing excess measurements, which can be tweaked with the N_{\max} option in the configuration file. This limit depends on the amount of functionality added to the buoy, but as all memory is statically allocated, the compiler will not compile the program if the memory limit is exceeded. In case the buoy is unable to find a base station until the controller memory is full, the oldest measurement is dropped from memory. The dropped readings can be recovered from the SD card on request from the base station, as each message contains an increasing measurement number to help keep track of untransmitted measurements.

Afterwards, the OLB buoy enters the *measuring and transmission* mode, which is a loop that repeats until the buoy either breaks, runs out of power, or is deactivated manually after recovery. The buoy will take measurements at a fixed or adaptive rate. The default measurement frequency f_d , as well as the minimal measurement frequency f_{\min} and the maximal measurement frequency f_{\max} can be set by the user in the configuration file prior to deployment. During each measurement cycle, the buoy performs n_m readings of each component, before averaging these values down to a single measurement value. If the *remove outliers* flag is set to true, then a σ -filtering is performed, where all readings more than σ_t standard deviations away from the mean are discarded. Furthermore, the *measurement frequency* can be modified remotely via the base station. We also provide a rudimentary adaptive measurement frequency for the buoy: If this feature is activated, the measurement frequency f is computed as a function of the GPS-measured speed v according to the following formula:

$$\frac{1}{f} = \begin{cases} \min\left(\frac{d_{\text{target}}}{v}, \frac{1}{f_{\min}}\right), & v > v_t, \\ f_d, & \text{else,} \end{cases} \quad (1)$$

where v_t is the adaptation threshold speed and d_{target} is the desired distance between each measurement. To avoid a buoy deadlock under weather conditions that make it difficult (or impossible) to get a GPS fix, the measurement cycle terminates if no GPS fix has been obtained within a time span of T_{GPS} .

The buoy will attempt to send the measured data to a base station during the transmission phase. The transmission phase occurs when both the minimum transmission period T_t has been exceeded and a minimum of N_m measurements have been stored in memory. In this phase, the buoy will look for signals from a base station (in listening mode at the frequency f_r), and if found, perform a handshake to verify that it can start transmitting. Afterwards, it will transmit (at transmission frequency f_t) as much of its stored data as possible within the timespan allotted to it by the base station. Finally, the buoy will switch back into listening mode to receive updates from the base station. A detailed overview of the LoRa protocol is given in Section 5. The configuration file includes several options to tailor the LoRa communication, including options to change the bandwidth B_L , spread factor s_f , coding rate c_r , output power W_{LoRa} and transmission and receiving frequencies (f_t and f_r respectively).

The buoy will also regularly transmit a beacon message. These messages include the buoy ID, and the most recently measured position and its corresponding timestamp. These messages are broadcast without a handshake and at a given frequency f_b , and can be received by a base station which is in recovery mode.

At the end of the loop, the buoy powers down any components it used during the loop, going into low-power sleep mode until it is time to perform a new measurement or transmission.

3.5 Buoy Housing and Buoy Design

There is no default buoy housing for the OLB buoy. In our deployments, a buoy hull was constructed using a combination of polypropylene (PP) plastic pipes. The LoRa antenna and thermometer are led through the buoy hull using cable glands. To decide on a hull size, the minimum requirement is that it contains the printed circuit board (PCB), with dimensions $63.3 \times 35.2 \times 34.2$ mm. In our development, we chose to use a combination of PP plastic pipes bought at a common hardware store. The container consisted of four pipe parts, a 75 mm diameter lid, a 75 mm pipe connector, a 75 to 50 mm narrower, and a 50 mm diameter lid. In the top 75 mm lid, two holes were drilled, one hole for a cable gland for the antenna and another, smaller hole for the thermistor string. All rubber bands in the cable glands were lubed with maritime grease to reduce the risk of leakage. The narrow bottom part of the container was used as a ballast compartment. Around the top, we also fastened small styrofoam disks to ensure that the buoys were stable and always on the surface. An image of an assembled buoy is shown in Figure 3.

An important note is the height of the antenna. The antenna included with the Wio-E5 Mini board, which we have used in the OLB buoy, is 19 cm long. As the LoRa range is severely reduced if the Fresnel zone is blocked [Yim et al., 2018, Coleman and Westcott, 2018], it is important to maximize the height of the antenna. From our practical experience with the hardware assembly, the included antenna has a combining joint 4 cm above the bottom, which is a structural weak point. Having this joint above the cable gland will weaken the joint, as the cable gland will need to be as tight as possible. This weakening might cause the hull to leak and potentially a loss of the buoy. Furthermore, this is also a constraint on how low one can place a base station without problems, as placing the base station too low might lead to significant portions of the Fresnel zone being blocked by the presence of ocean waves.

4 Base Station Components

The second component of the OLB framework is the base station, which acts as an intermediately between the OLB drifters and the cloud, receiving messages from the drifters and uploading these to the cloud from where the data can be

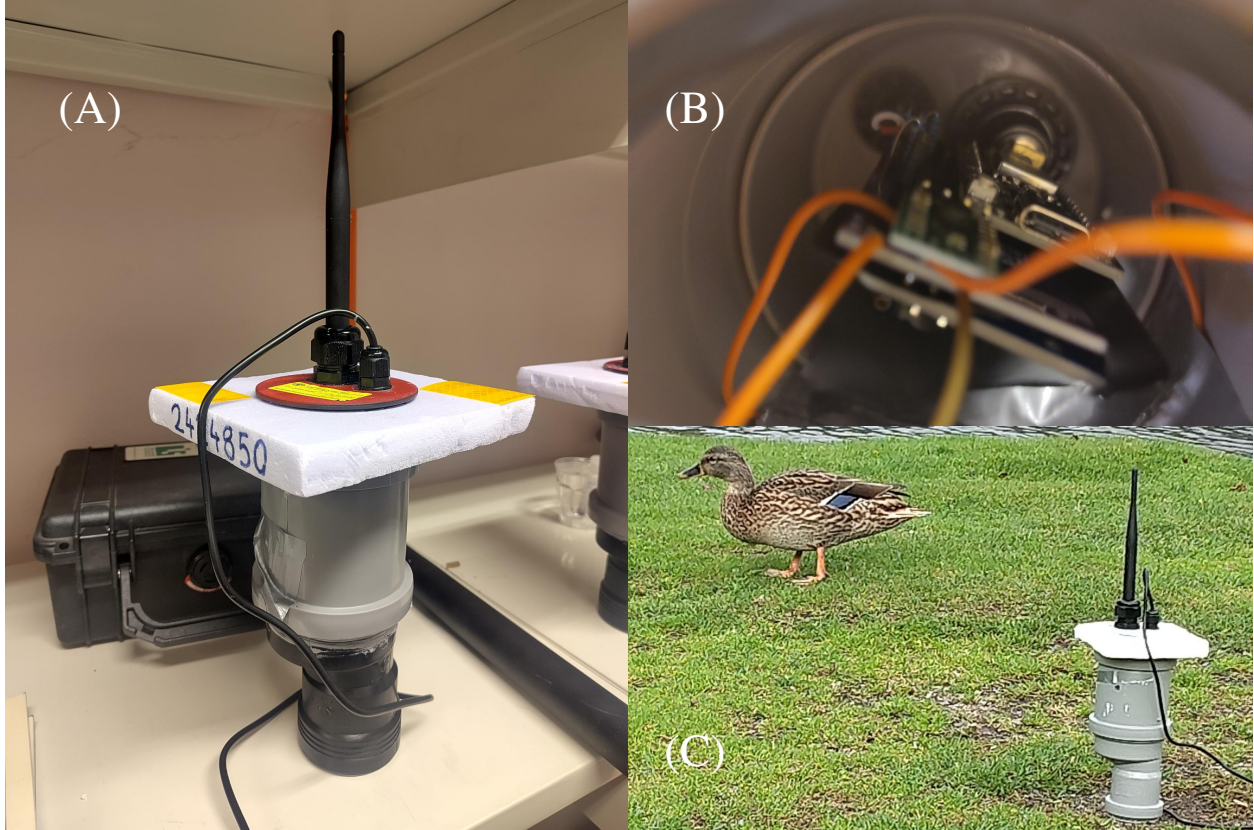


Figure 3: An assembled OLB buoy in a container with a PCB (subfigure A), and the inside of the buoy (subfigure B). Subfigure (C) shows the buoy alongside a female *Anas platyrhynchos* (mallard duck) near Sognsvann, Oslo.

downloaded. The base station consists of a radio transceiver which communicates with the buoys, an SD card writer and a GSM module which transmits the received data to a cloud frontend.

The OLB base station is, as the buoy, controlled by a Wio-E5 Mini board [Seeed Studio, 2023], which acts as main processor and LoRa transceiver to operate the base station and to receive measurements and send instructions to the OLB drifter. The base station is also equipped with a Blues Notecarrier A module [Blues Inc], which periodically transmits the received data from the buoy to the cloud via GSM. As the data platform for our cloud frontend, we use notehub.io, which can receive, at the time of writing, 5000 messages (with a maximum message size of 1 MB) for free each month and charges 11.5 USD per 15000 messages thereafter. To minimize the amount of messages sent to the cloud, the base station stores and bundles several buoy messages into a single data packet before transmitting. Each base station is equipped with a unique base station ID, which it broadcasts at regular intervals. A schematic for the base station layout is shown in Figure 4.

The base station uses Notecard to enable the remote management of deployed buoys. The Notecarrier integration with Notehub allows a user to remotely send instructions to the base station, and these can be forwarded to individual buoys, as described above. For instance, a signal can be sent to the base station to reset itself in the event of a software error. Furthermore, it is possible to request a specific measurement from a specified buoy; this request will be forwarded from the base station to the given buoy.

The OLB base station also comes equipped with local storage capabilities in the form of an SD card writer of the same kind as the one used by the buoy. As notehub, the data platform to which the Notecard sends the data, only keeps the data for a period of three days, so this local storage is a crucial fail-safe in case the data export pipeline from notehub were to fail either due to human or code error. The Adafruit SD writer works well for this purpose as it is able to operate at both a 3.3 V logic level, used by the buoys, and at a 5 V level, used by the base station. In our tests, we used three 13 Ah 3.6 V Lithium Batteries as the power source for the base station, which were regulated up to a 5 V logic level

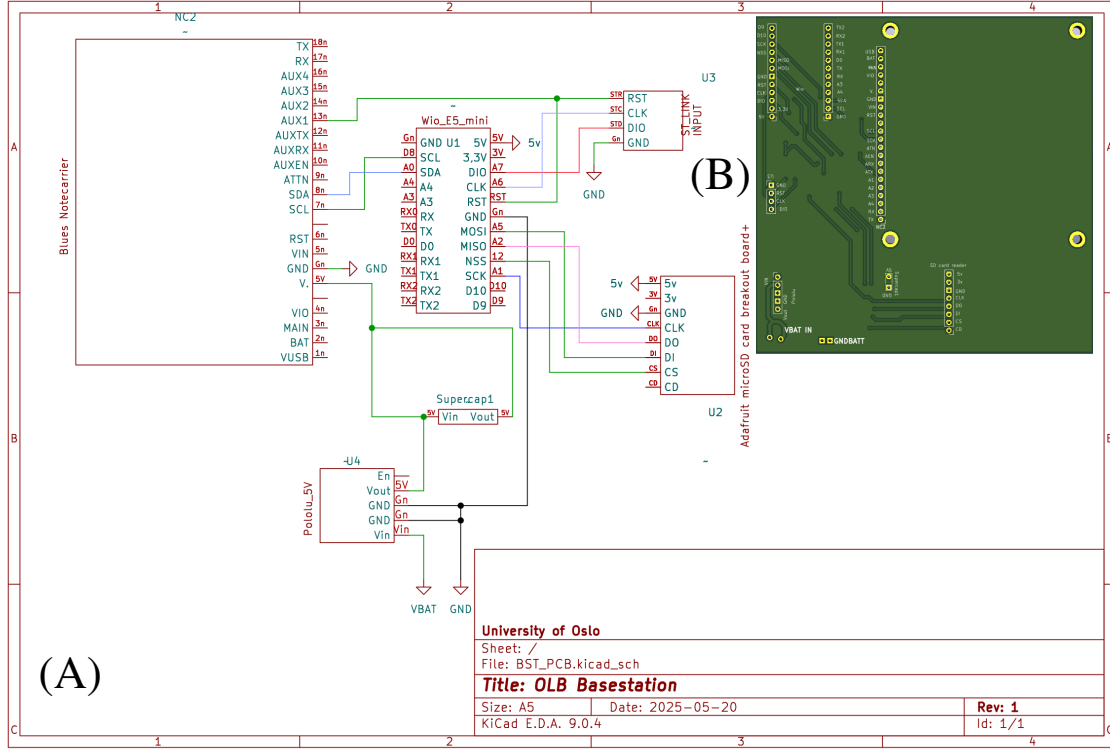


Figure 4: The wire schematic for the base station [Subfigure (A)] and the corresponding PCB layout [Subfigure (B)]. The Wio-E5 Mini board acts as the radio transceiver and main control unit. The system operates on 5V logic, and can be reset remotely from the notecarrier.

using a Pololu step-up/step-down voltage regulator [Pololu Robotics and Electronics, b]. A full component list with an approximate price tag can be seen in Table 5.

5 Data Transmission Protocol

The OLB buoy uses LoRa to send messages to the base station. LoRa uses radio messages on a low frequency band (433 MHz and 868 MHz in the EU) with a range of a few kilometres (a detailed overview of LoRa is given by Devalal and Karthikeyan [2018]). Hence, any deployment of an OLB buoy requires the deployment of base stations around the area of interest. To ensure that messages are not lost due to low base station coverage, we implemented the following protocol (for a visual representation, see Figure 5):

- Step 1:** The base station transmits its ID and listening frequency $f_{b,r}$ at a predefined transmission frequency $f_{b,s} = 434$ MHz. The listening frequency transmitted to the base station is unique for each base station, to avoid possible data duplication by having more than one base station receive data from the same buoy simultaneously.
- Step 2:** The base station switches to a listen mode at its own unique listening frequency frequency $f_{b,r}$. If a buoy manages to catch the transmitted ID and has a sufficient amount of data for transmission, it will respond by transmitting a *ready* signal consisting of the base station ID and the buoy's unique ID.
- Step 3:** If the base station receives a *ready* signal from a buoy which contains the base station's ID, it will transmit a *go ahead* message at $f_{b,s}$ containing the base station ID, the buoy ID and the amount of time that the base station will listen for messages from the buoy. The buoy will read back the *go ahead* message from the base station and start to transmit if the base station and buoy IDs both match the handshake transmitted in Step 2.
- Step 4:** The buoy transmits data to the base station until the buoy either has transmitted all of its available data or the allotted listen time (minus a certain grace period to avoid an overshoot) from the base station runs out.

Component	Function	Producer	Price (per 08-2025) [USD]
Wio-E5 Mini	Main controller unit, radio transceiver	Seeed studio	21.90
Notecarrier	GSM module carrier	Blues	25
Notecard	GSM module	Blues	63
Micro-SD card	SD card writer/reader	Adafruit	7.50
breakout board+ Pololu 5V S7V8F3	Step up/down voltage regulator	Pololu	17.95*
SD card	Data storage	Adafruit	9.95
3 Saft LSH 20	13 Ah Li-battery	Saft	54*
PCB	Correct wire connection between components	JLCPCB	1-6*
Container parts	Waterproof BST container equipment	-	~15
Price per base station			213

Table 5: The hardware components of the OLB base station, their function and manufacturer. For convenience, manufacturer names are hyperlinked to the product page where the components were ordered. Prices marked with an asterisk (*) are subject, at the time of writing, to a bulk order discount. In particular, the cost of a PCB is almost exclusively shipping, and the price listed is a price estimate for a single PCB out of an order of 5–30 PCBs. Hence, the final price might be lower than what is listed here for several of the components.

Step 5: After the buoy has finished transmitting data within the allotted listening time, the buoy transmits an *end* message before switching the radio to listening mode. This message is read by the base station, which then allows the base station to transmit new directives to the buoy. These directives include updates to the mutable parameters in Table 1, or requests for packages that were lost in transit. As each measurement has a unique measurement ID and is stored on the onboard SD card, the base station only needs to transmit the ID of the requested measurement to the buoy for it to retransmit the measurement.

The protocol ensures that the buoy will not try to send any data (which is then, upon successful transmission, deleted from system memory) unless it has received a recent confirmation of having a base station within listening range. The transmitted data are encoded as a raw byte array before transmission to minimize the amount of data needed to transmit a single measurement.

6 Validation

To validate the OLB framework, we performed a number of experiments with the OLB framework. First, to determine the range limits of the distance between the base station and the buoy, we performed range experiments. These were performed in the ocean or across lakes, to ensure that our experiments closely resemble the in situ conditions that the buoys will encounter. Second, to determine the buoy’s ability to continue to operate in water, we performed reliability experiments. These experiments demonstrated that the OLB buoy can operate for several months in ocean conditions.

6.1 Transmission Range Experiments

Setup. We performed three experiments with the aim of establishing an estimate on the effective range of the LoRa communication between a base station and a buoy. Two experiments were performed outdoors near a lake with one or more buoys and one base station. The buoy(s) were mostly configured with the standard configuration, but to make the experiments practical they were given a reduced measurement period $T_m = 15$ s and a minimum transmission period $T_t = 15$ s. The measurements per transmission were $N_m = 4$. Hence, the buoy would try to send a message roughly every minute. In each experiment, the base station was placed at a known location while the buoy was carried around the lake. During the first range experiment, at *Sognsvann* lake, the buoy position at the time of transmission was validated using a Garmin Forerunner 255s watch. In combination with the timestamp of the message received from the base station, this ensured that we were able to compute the exact distance between the sender and receiver. The second range experiment, at *Nøklevann* lake, focused on transmission distance. The experiment was only performed at two discrete distances due to the heavy foliage and distance between the road and the lake for most of the trip. The third range experiment, in the *Oslofjord*, was performed with a base station placed at a vantage point on land while the drifter was pulled by a boat in a straight line until we lost contact with the base station. In all experiments, the handshake was enabled to ensure that transmissions would occur only if the buoy was within range of the base station.

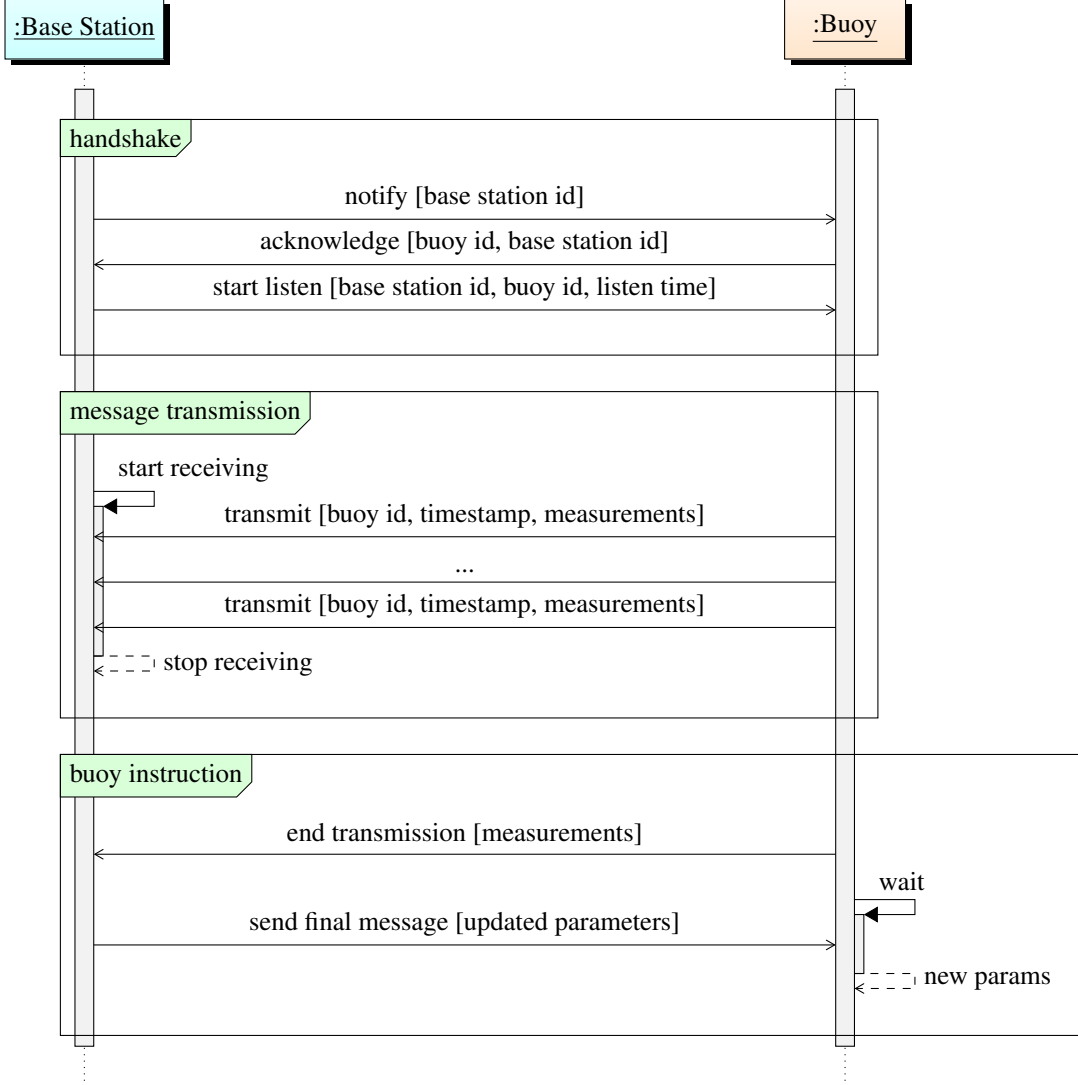


Figure 5: Radio protocol between base station and buoy. The protocol is separated into three stages. The base station is, when not busy, regularly sending out a short message notifying buoys in the area that it is available for data reception. Once a buoy is ready to transmit, it will turn on the radio to listen mode and check if it gets a signal from a base station. If so, the buoy and the base station will perform a handshake to ensure that the connection is stable and to avoid multiple buoys transmitting simultaneously. Once verified, the base station enters listening mode while the buoy transmits as much data as possible within the time allotted to it by the base station. Finally, the buoy sends a message confirming it is done to the base station before switching to listening mode. If received, the base station might send updated directives to the buoy.

Results. The connection was maintained throughout the *Sognsvann* experiment, with some exceptions in areas with dense foliage. The coordinate of each transmission is shown in Figure 6A. In the figure, the blue dots show the closest position in time of the exercise watch to a successful transmission from the buoy. The longest observed transmission range was ~ 1.2 km. In the *Nøklevann* experiment, we were able to get a stable transmission between the buoy and the base station along both the short side and the long side of the lake. The positions in this experiment are shown with blue (long side experiment) and red (short side experiment) asterisks in Figure 6B. The distance between the sender and receiver was 1.3 km along the short side and 2.3 km along the long side of the lake, although the base station had to be placed in a manner that minimized the amount of foliage between the two. In the *Oslofjord* experiment, we observed a maximum range of 1.8 km before communication was lost, as shown in Figure 6C. The results are summarized in Table 6.

Location	Max. range [km]	In water
Sognsvann	1.2	No
Nøklevann	2.3	No
Oslofjord	1.8	Yes

Table 6: Observed ranges from the different range experiments. The “In water” column indicates if the buoy was floating in water or hand held during the experiment.

6.2 Buoy Longevity and Reliability Experiments

Setup. We performed two experiments to validate the longevity and reliability of the OLB design. The first experiment focused on the buoy’s reliability faced with long-term exposure to oceanic conditions, while the second experiment addressed the stability of the communication between each component. For the first experiment, we prepared two buoys with default configuration parameters (shown in Tables 1 and 2). The two buoys were then moored to a communal underwater garden at Nesoddtangen. A base station was placed on a vantage point nearby (approximate distance 30 meters). An image from the deployment of an earlier prototype in the same location is shown in Figure 7B. The buoys were moored by attaching a rope to the top rope of the underwater garden at two meters depth, and deployed on Thursday May 8, 2025. The second experiment was performed starting on October 2, 2025. Here, one buoy was initialized with a low measurement period $T_m = 20$ s, the other parameters being the default values from Tables 1 and 2. This buoy was placed in a laboratory and a base station with the default parameter configuration was placed beside the buoy. After two weeks, the buoy was powered off for three hours before being it was repowered, and two hours later the base station was powered off for three hours before being repowered.

Results. The first reliability experiment, where two buoys were moored outside Nesoddtangen, demonstrated that the buoys functioned for a months time. The recorded temperature by both buoys is shown in Figure 7. The experiment did suffer from frequent loss of connection between the base station and the cloud due to an issue in the notecarrier in which it would enter sleep mode after a certain amount of time. This issue motivated the second test of the connection stability, which was performed after this issue had been solved. The second laboratory test found no signs of the base station entering an undesired sleep mode, with a stable connection for more than two weeks (data not shown).

6.3 Testing the Interaction Between Multiple Buoys and Base Stations

Setup. We performed a test with the aim of checking if several base stations and buoys would interfere, and if the buoys would exhibit some sort of base station preference. To this end, we deployed two base stations on opposite ends of *Sognsvann* lake. Two buoys were activated, with a packet count threshold of 3, and measurement period $T_m = 15$ s. The two base station locations were placed approximately 1.2 km from each other. The buoys were then walked from base station A to base station B alongside the eastern side of the lake, with one thermometer measuring the air temperature and the other being held in hand under a glove, ensuring a measurable difference in temperatures. Once the buoys were by base station B, the researcher at base station A picked up the base station and carried it back to base station B along the western side of the lake.

Results. The messages from the buoys did not interfere or get mixed up by the base station, as the *warm* and *cold* buoys were at no point mixed up in the signals (data not shown). Furthermore, there is little discernible difference in preference between the two base stations, showing that there is no implicit discrimination of base stations from the buoys end. Hence, the handshake acts as the check to see if the connection between buoy and base station is sufficient for communication, as was expected.

6.4 A Live Deployment in the Drammensfjord

Setup. We assembled 16 OLB buoys and 8 base stations that were used for a first field experiment in the *Drammensfjord*. The aim of the experiment was twofold, we wanted to both test the OLB solution in field conditions while simultaneously measuring and collecting data on the fjord circulation as the ecological conditions in the entirety of the greater Oslo fjord is critical [Frigstad et al., 2025]. The base stations were deployed at the locations marked with a green marker in Figure 8A and B. The buoys were deployed from a bridge at the southern bifurcation of the Drammen river close to the estuarine outlet. The buoys were coded with the standard parameter configuration in Table 1, except for a reduced measurement period $T_m = 5$ min. Figure 8C shows the deployment procedure, Figure 8D a buoy drifting into the fjord and Figure 8E a base station deployed at a strategic vantage point close to the fjord.

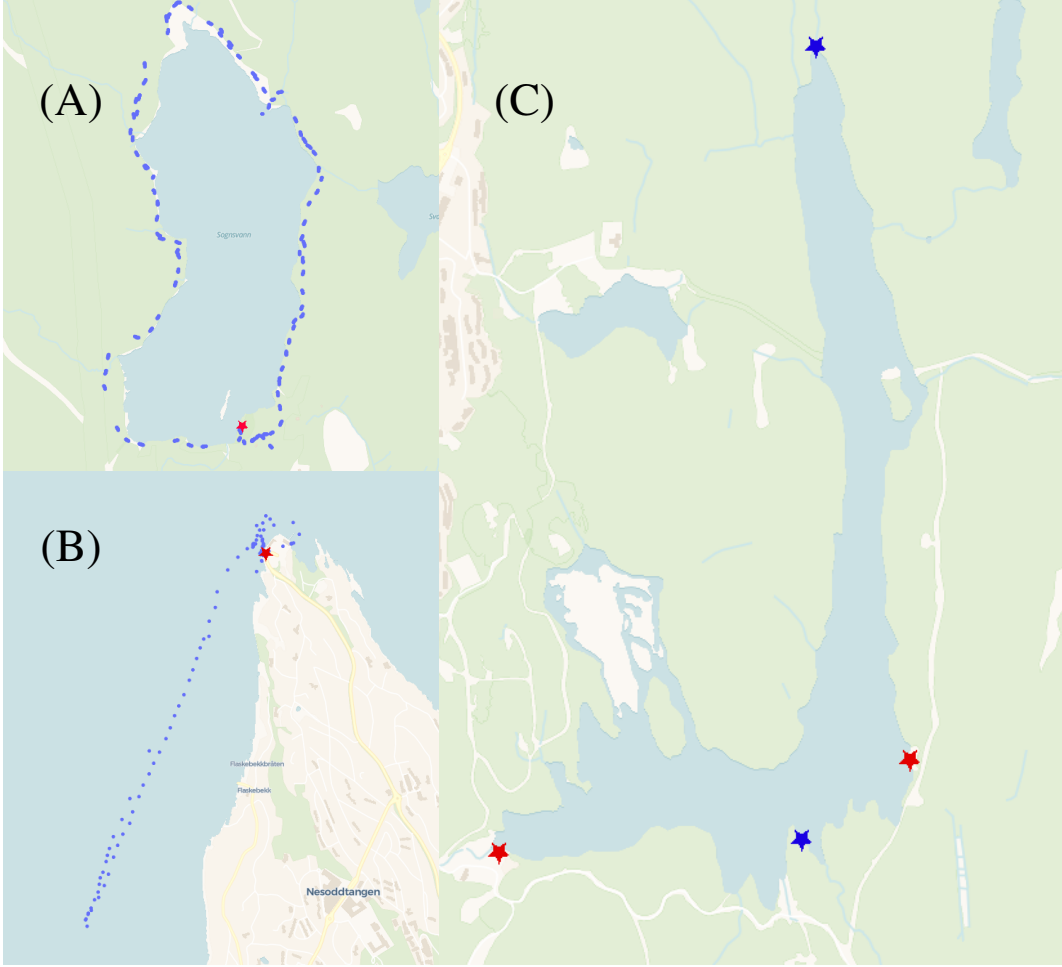


Figure 6: The performed transmission range experiments. Subfigure (A) shows the position of the buoy at the time it managed to establish a connection with the base station during the *Sognsvann* range experiment. Each blue dot shows the measured position of the exercise watch at the timestamp of a confirmed transmission from the carried buoy. The position of the base station is marked by a red asterisk. The longest measured transmission distance was ~ 1.2 km. Subfigure (B) shows the location of the sender/receiver at the two sampling points at *Nøklevann*. The distance between the two red asterisks (located at the south east and south west of the lake) is 1.3 km, while the distance between blue asterisks (located at the southern and northern part of the lake) is 2.3 km. Subfigure (C) shows the trajectory taken by a buoy pulled by a boat in the *Oslofjord*, the base station location is marked by a red asterisk.

Results. Of the 16 deployed buoys, we were able to recover the remote particle trajectories of 12 buoys (either in full or in part). Furthermore, we were able to recover 8 of the deployed buoys, with the remaining 8 either having lost signal before hitting shore, or hitting shore at locations that were too difficult to reach for a safe recovery to be possible. From the recovered buoys, we were able to obtain the raw data from 7 of the 8 onboard SD cards. The obtained SD card trajectories are shown in Figure 8A, while the transmitted trajectories are shown in Figure 8B. The maximal measured transmission distance during this deployment was 5.3 km.

The majority of the measurements ($\sim 70\%$) were taken in the desired $T_m = 5$ min interval, but a significant number ($\sim 30\%$) were taken with a large time interval in between measurements. The distribution of these measurements is shown in Figure 9. Different buoys exhibited clear differences in reliability, most notably Buoy 1572911 measured predominantly on time, while Buoy 2824859 only sporadically measured on time, with the majority of GPS fixes taking close to about 20 minutes to get, suggesting that care should be made during assembly, as human error might adversely affect buoy performance.

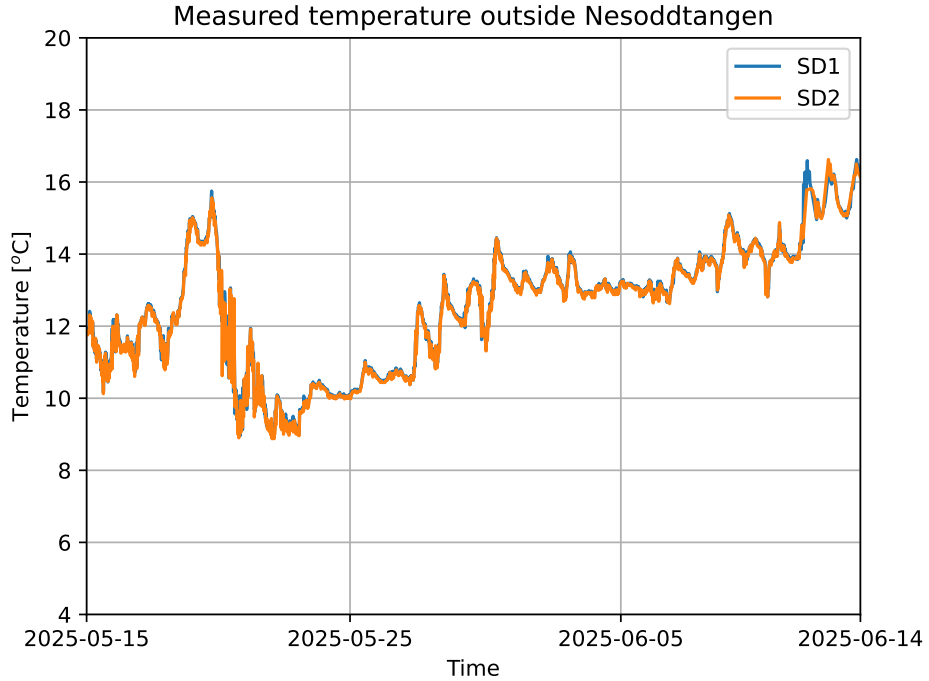


Figure 7: Temperature measurements outside of Nesoddtangen, recovered from two onboard SD cards. The buoys were deployed on May 15, 2025, and moored to an underwater installation, hence being subjected to oceanic conditions for the entirety of the measurement period.

7 Discussion and Conclusion

The OLB framework is a complete system package to measure oceanographic flows in coastal and fjord environments. A base station can handle multiple buoys during a given deployment, and the battery lifetime has been shown to exceed three months in the field. Furthermore, the comparatively low price of 100 USD/buoy makes it possible to acquire many buoys for a field experiment within a constrained budget. Hence, the OLB would be suited for capturing spatial variance in flow patterns, as well as getting an estimate for ensemble statistics of the measured flow. The greatest limitation of the OLB is its transmission range, with an observed upper bound of 5 km, which might be lower in the presence of waves. This limitation makes the OLB less suitable for measurements in the open ocean far from the coast, as it would be challenging to obtain sufficient coverage from the base stations. A moored installation further offshore should be possible to construct, following the example of [Raphael et al. \[2025\]](#).

The OLB buoy as a device can perform similar measurements as previously developed buoys, such as [da Silva et al. \[2022\]](#), [Majumder et al. \[2024\]](#), [Raphael et al. \[2025\]](#) and [SmartOcean \[2016\]](#). However, the OLB buoy stands out in its open-source aspect. The source code, hardware, and data platform are publicly available and modifiable under a permissive license. Open-source instrumentation has several distinct advantages. Similarly to, e.g. the OpenMetBuoy [\[Rabault et al., 2022\]](#), the SFY [\[Hope et al., 2025\]](#) and microSWIFT [\[Thomson et al., 2024\]](#), the OLB buoy is fully usable out of the box at the cost price of assembling the buoy. Furthermore, since both the code and hardware are openly available, open buoys such as OLB also serve as a solid starting point for users whose needs are almost or somewhat covered by the existing designs. Open-source instruments are also able to strengthen their own source code and hardware through community feedback, since all relevant information is publicly available, strengthening confidence in the solution in the long term.

The OLB buoy has been shown to be stable over long time periods and to be energy efficient. With more than three months (in the worst case scenario) of continuous operation on a single 13 Ah lithium battery, we can reasonably assume that the OLB buoys have sufficient battery lifetime to last for most drifter-in-fjord deployments due to the requirement for the buoys to be close to a coast with mounted base stations. For moored and long-time deployments, additional battery capacity can be obtained simply by adding more batteries to the buoy. Several power consumption optimizations have been applied to extend battery lifetime, and we are continually working to improve this aspect

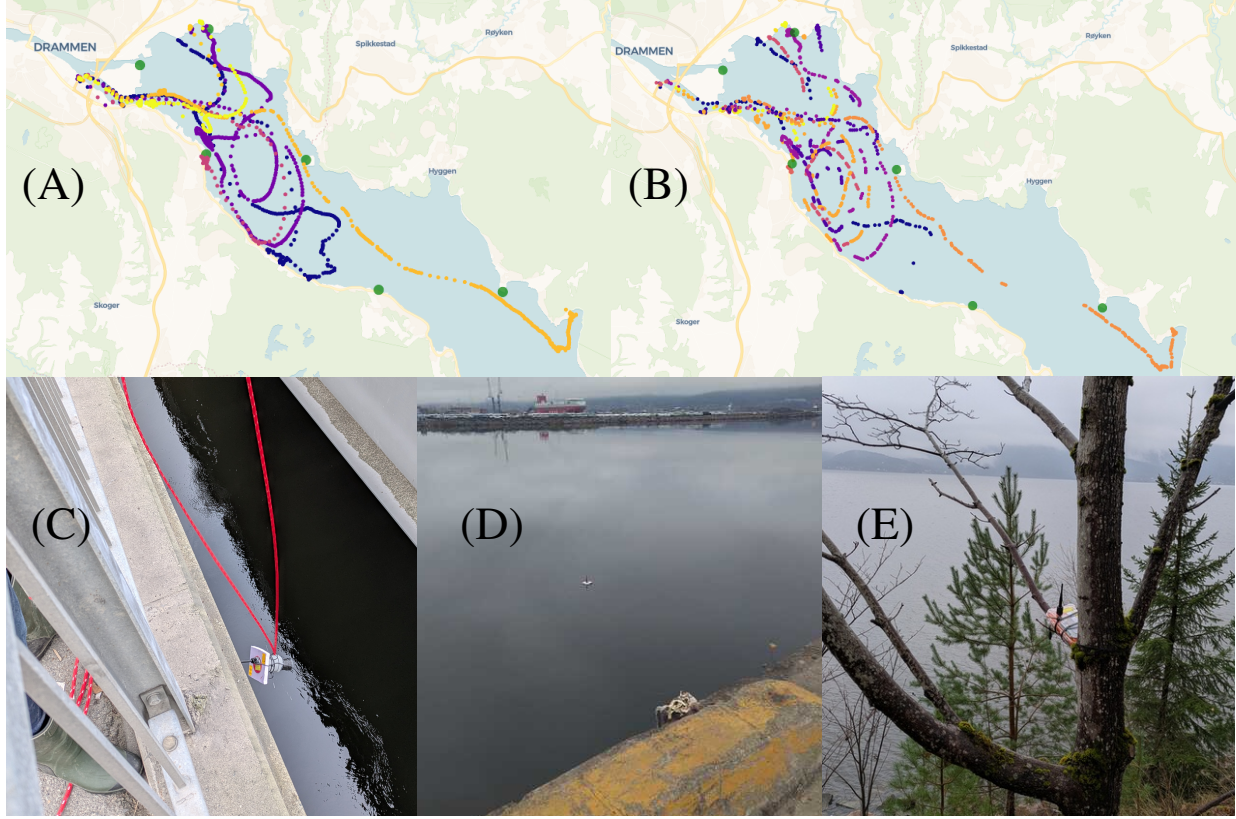


Figure 8: The observed trajectories from the *Drammensfjord* deployment, alongside some illustrations of the deployment. Subfigure (A) show the recovered trajectories from the onboard SD card, while Subfigure (B) show the buoy coordinates that was received by a base station. The trajectories are colour coded by buoy ID. Subfigures (C) to (E) show the deployment of a buoy into the Drammen river (C), a buoy drifting into the fjord (D) and a base station at a vantage point (E).

further where possible. In combination with the moderate price tag of ~ 100 USD, this means the OLB buoy is a viable low-cost alternative to commercial and closed-source buoys if the targeted use case lies within the range constraints of LoRa technology.

The OLB buoy, as described in this paper, is an open instrument that is still under development, and extensions to different sensors and use cases are developed. For example, work has already been done on a turbidity sensor library, with applications to permanent moored sensors in mind. Furthermore, all data that we gather using the OLB buoy will also be made publicly available. This will allow for easier validation of coastal ocean models in general and of fjord environments in particular. The comparatively low price allows for a greater statistical representation of the surface drift, making it easier to validate a numerical model against observed patterns. Furthermore, with the increasing number of digital twin infrastructure initiatives for ocean monitoring (e.g. [Chen et al. \[2023\]](#), [Tzachor et al. \[2023\]](#)) and work with trace DNA (e.g. [Shelton et al. \[2022\]](#)), this information is also valuable outside of oceanography.

Acknowledgements

This work was supported by the Sustainability initiative of the University of Oslo and the Digital Arctic Twins network (DART, funded by the University of the Arctic). The authors thank Lars Dalen and Marinreparatørene for inviting us to use their communal underwater garden at Nesoddtangen for validation experiments, as well as for helping us to deploy and recover the buoys. We also thank Issam Rais at the Arctic University of Tromsø for his help and code review during a hackathon at Marinreparatørene, and Olav Gundersen at the Hydrodynamical Laboratory at the Department of Mathematics at the University of Oslo for his assistance in the workshop with buoy construction. A special thanks goes to Ivar Vannebo and Morten Hansen at Drammen Havn and Hans Martin Hansen for letting us install base stations

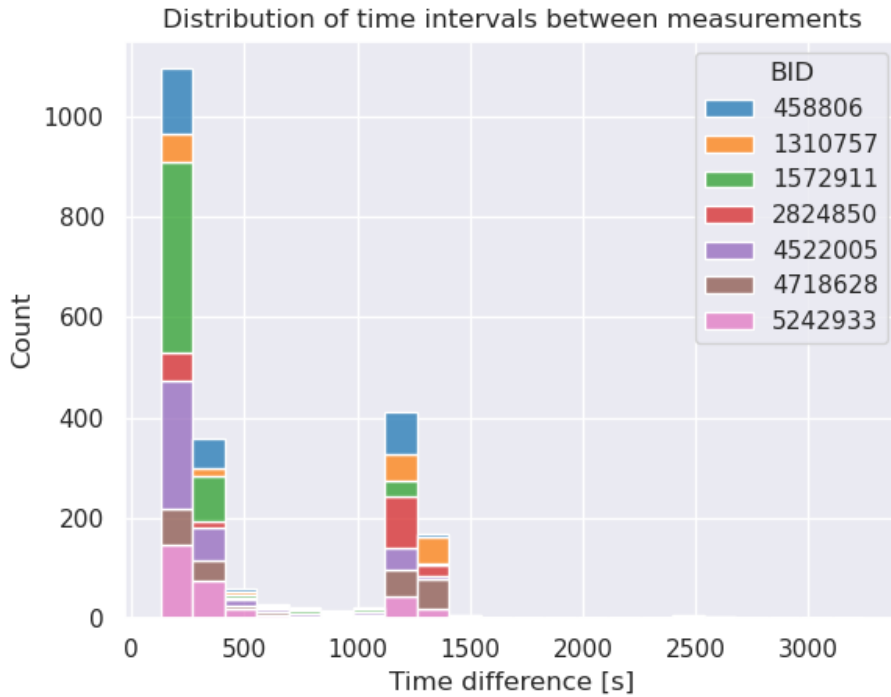


Figure 9: The time interval distribution of GPS measurements. Each colour represent one recovered buoy, with the shown data being retrieved from the onboard SD card. Four time intervals were above one hour, and have been cut from the figure for legibility.

at their premises, and assisting us with the *Drammensfjord* experiment. Finally, we thank Daniel Sæther and Tor Erik Kristiansen for assisting us in recovering the buoys once they had drifted ashore.

References

Adafruit. Adafruit ultimate GPS breakout - pa1616s, 2014. URL <https://cdn-shop.adafruit.com/datasheets/GlobalTop-FGPMMPA6H-Datasheet-V0A.pdf>. Last visited: 08/12-2025.

Adafruit. Adafruit MicroSD breakout board+, 2025. URL <https://www.adafruit.com/product/254>. Last visited: 08/12-2025.

Meisam Amani, Armin Moghimi, Seyed Mohammad Mirmazloumi, Babak Ranjgar, Arsalan Ghorbanian, Saeid Ojaghi, Hamid Ebrahimi, Amin Naboureh, Mohsen Eslami Nazari, Sahel Mahdavi, et al. Ocean remote sensing techniques and applications: A review (part i). *Water*, 14(21):3400, 2022. doi:[10.3390/w14213400](https://doi.org/10.3390/w14213400).

Mohamed Aref and Axel Sikora. Free space range measurements with Semtech Lora™ technology. In *2014 2nd international symposium on wireless systems within the conferences on intelligent data acquisition and advanced computing systems*, pages 19–23. IEEE, 2014. doi:[10.1109/IDAACS-SWS.2014.6954616](https://doi.org/10.1109/IDAACS-SWS.2014.6954616).

Blues Inc. Blues Notecarrier A, 2025. URL <https://dev.blues.io/datasheets/notecarrier-datasheet-notecarrier-a/>. Last visited: 26/08/2025.

Luigi Cavalieri, Victor Alari, Alvise Benetazzo, Jan-Victor Björkqvist, Øyvind Breivik, Jacob Davis, Gaute Hope, Atle Kleven, Frode Leirvik, Tor Nordam, et al. More room at the top: How small buoys help reveal the detailed dynamics of the air-sea interface. *Bulletin of the American Meteorological Society*, 106(6):E1063–E1076, 2025.

Ge Chen, Jie Yang, Baoxiang Huang, Chunyong Ma, Fenglin Tian, Linyao Ge, Linghui Xia, and Jianhui Li. Toward digital twin of the ocean: From digitalization to cloning. *Intelligent Marine Technology and Systems*, 1(1):3, 2023. doi:[10.1007/s44295-023-00003-2](https://doi.org/10.1007/s44295-023-00003-2).

David Coleman and David Westcott. Radio frequency signal and antenna concepts. In *CWNA: Certified Wireless Network Administrator Study Guide*, pages 139–142. Wiley & Sons, Inc, 2018. doi:[10.1002/9781119549406.ch5](https://doi.org/10.1002/9781119549406.ch5).

António Jorge da Silva, Alexandre Sousa, Félix Pedrera, Joaquín del Río Fernández, José P. Pinto, M Oliveira, Pedro Gonçalves, Philippe de Saint Léger, and Rogério Chumbinho. Generation WAVY: a new breed of surface drifters for all ocean domains. In *7as Jornadas de Engenharia Hidrográfica*, pages 359–362. Instituto Hidrográfico, 2022. URL <https://hdl.handle.net/2117/369944>.

Datawell BV. Datawell waverider reference manual. *Datawell BV, Zumerlustraat*, 4:2012, 2006. URL <https://cdip.ucsd.edu/themes/media/docs/documents/pdf/mk3.pdf>.

Datawell BV. History of Datawell, 2011. URL https://datawell.nl/wp-content/uploads/2022/10/datawell_jubileumboek_english.pdf. Last visited: 08/12-2025.

Shilpa Devalal and A Karthikeyan. LoRa technology - an overview. In *Second international conference on electronics, communication and aerospace technology (ICECA 2018)*, pages 284–290. IEEE, 2018. doi:[10.1109/ICECA.2018.8474715](https://doi.org/10.1109/ICECA.2018.8474715).

Reyhane Falanji, Martin Heusse, and Andrzej Duda. Range and capacity of LoRa 2.4 GHz. In *International Conference on Mobile and Ubiquitous Systems: Computing, Networking, and Services*, pages 403–421. Springer, 2022. doi:[10.1007/978-3-031-34776-4_21](https://doi.org/10.1007/978-3-031-34776-4_21).

Anthony Freeman, Victor Zlotnicki, Tim Liu, Benjamin Holt, Ron Kwok, Simon Yueh, Jorge Vazquez, David Siegel, and Gary Lagerloef. Ocean measurements from space in 2025. *Oceanography*, 23(4):144–161, 2010. URL <https://www.jstor.org/stable/24860869>.

Helene Frigstad, Paula Ramon, Gunhild Borgersen, Anette Engesmo, Andre Staalstrøm, Lars-Johan Naustvoll, Sarah Lerch, Merete Schøyen, Anders Ruus, Tore Strohmeier, Tone Falkenhaug, Carla Freitas, Even Moland, Thrond Oddvar Haugen, Siv Hoff, Sissel Jentoft, Tor Atle Mo, Eli Rinde, Sveinn Are Hanssen, Viviam Husa, Henning Steen, and Mats Walday. Miljødirektoratet, 2025. ISBN 978-82-577-7773-9. URL <https://www.miljodirektoratet.no/publikasjoner/2025/januar-2025/tilstandsrapport-for-oslofjorden/>.

Oliver B Fringer, Clint N Dawson, Ruoying He, David K Ralston, and Yinglong Joseph Zhang. The future of coastal and estuarine modeling: Findings from a workshop. *Ocean modelling*, 143:101458, 2019. doi:[10.1016/j.ocemod.2019.101458](https://doi.org/10.1016/j.ocemod.2019.101458).

Bruce Hackett, Øyvind Breivik, and Cecilie Wettre. Forecasting the drift of objects and substances in the ocean. In *Ocean weather forecasting: an integrated view of oceanography*, pages 507–523. Springer, 2006. doi:[10.1007/1-4020-4028-8_23](https://doi.org/10.1007/1-4020-4028-8_23).

Gaute Hope, Torunn Irene Seldal, Jean Rabault, Helge Thomas Bryhni, Patrik Bohlinger, Jan-Victor Björkqvist, Tor Nordam, Atle Kleven, Arsalan Mostaani, Birgitte Rugaard Furevik, Lars Robert Hole, Roger Storvik, and Øyvind Breivik. SFY — a lightweight, high-frequency, and phase-resolving wave buoy for coastal waters. *Journal of Atmospheric and Oceanic Technology*, 42(2):133–154, 2025. doi:[10.1175/JTECH-D-23-0170.1](https://doi.org/10.1175/JTECH-D-23-0170.1).

Robert Howarth, Donald Anderson, James Cloern, Chris Elfring, Charles Hopkinson, Brian Lapointe, Tom Malone, Nancy Marcus, Karen McGlathery, Andrew Sharpley, and Dan Walker. Nutrient pollution of coastal rivers, bays, and seas. *Issues in ecology*, 7:1–16, 2000. URL <https://www.esa.org/esa/wp-content/uploads/2013/03/issue7.pdf>. Last visited: 08/12.15.

Alison L. Kohout, Bill Penrose, Scott Penrose, and Michael J.M. Williams. A device for measuring wave-induced motion of ice floes in the Antarctic marginal ice zone. *Annals of Glaciology*, 56(69):415–424, 2015. doi:[10.3189/2015AoG69A600](https://doi.org/10.3189/2015AoG69A600).

Konstantin Korotenko, Malcolm J. Bowman, and David E. Dietrich. High-resolution numerical model for predicting the transport and dispersal of oil spilled in the Black Sea. *Terrestrial, Atmospheric & Oceanic Sciences*, 21(1), 2010. doi:[10.3319/TAO.2009.04.24.01\(IWNOP\)](https://doi.org/10.3319/TAO.2009.04.24.01(IWNOP)).

Matthieu Le Hénaff, Vassiliki H. Kourafalou, Claire B. Paris, Judith Helgers, Zachary M. Aman, Patrick J. Hogan, and Ashwanth Srinivasan. Surface evolution of the Deepwater Horizon oil spill patch: combined effects of circulation and wind-induced drift. *Environmental science & technology*, 46(13):7267–7273, 2012. doi:[10.1021/es301570w](https://doi.org/10.1021/es301570w).

Kris Maine, Carrie Devieux, and Pete Swan. Overview of IRIDIUM satellite network. In *Proceedings of WESCON'95*, page 483. IEEE, 1995. doi:[10.1109/WESCON.1995.485428](https://doi.org/10.1109/WESCON.1995.485428).

Arnas Majumder, Michele Losito, Santhosh Paramasivam, Amit Kumar, and Gianluca Gatto. Buoys for marine weather data monitoring and LoRaWAN communication. *Ocean Engineering*, 313:119521, 2024. doi:[10.1016/j.oceaneng.2024.119521](https://doi.org/10.1016/j.oceaneng.2024.119521).

Andrew M. Moore, Hernan G. Arango, Gregoire Broquet, Brian S. Powell, Anthony T. Weaver, and Javier Zavala-Garay. The Regional Ocean Modeling System (ROMS) 4-dimensional variational data assimilation systems: Part I – system overview and formulation. *Progress in Oceanography*, 91(1):34–49, 2011. doi:[10.1016/j.pocean.2011.05.004](https://doi.org/10.1016/j.pocean.2011.05.004).

Malte Müller. Advancing coupled Arctic forecasting: Insights from the workshop on coupled modelling and observations in the marginal ice zone, 2025. URL <https://www.wwrp-pcaps.net/news/svalmizworkshop>. Last visited: 08/08-2025.

Malte Müller, Jean Rabault, and Cyril Palerme. Svalbard marginal ice zone 2024 campaign–cruise report. *arXiv preprint arXiv:2407.18936*, 2024. doi:[10.48550/arXiv.2407.18936](https://doi.org/10.48550/arXiv.2407.18936).

Malte Müller, Jean Rabault, Chiara De Geeter, Cyril Palerme, Bikas Chandra Bhattarai, Fabrice Collard, Steinar Eastwood, Sylvain Herlédan, Gaute Hope, Nicholas Edward Hughes, Marius O. Jonassen, Jørn Kristiansen, Frank Nilsen, and Olav Weisser. Svalbard Marginal Ice Zone 2024: A distributed network of temperature, waves, and sea ice drift observations. *Nat. Sci. Dat.*, 2025. doi:[10.1038/s41597-025-05889-7](https://doi.org/10.1038/s41597-025-05889-7).

Brenda L. Norcross and Richard F. Shaw. Oceanic and estuarine transport of fish eggs and larvae: a review. *Transactions of the American Fisheries Society*, 113(2):153–165, 1984. doi:[10.1577/1548-8659\(1984\)113%3C153:OAETOF%3E2.0.CO;2](https://doi.org/10.1577/1548-8659(1984)113%3C153:OAETOF%3E2.0.CO;2).

Jaime B. Palter. The role of the Gulf Stream in European climate. *Annual review of marine science*, 7(1):113–137, 2015. doi:[10.1146/annurev-marine-010814-015656](https://doi.org/10.1146/annurev-marine-010814-015656).

Silvano Porto Pereira, Paulo Cesar Colonna Rosman, José Luis Sánchez-Lizaso, Iran Eduardo Lima Neto, Rodrigo Amado Garcia Silva, and Melissa Rodrigues. Brine outfall modeling of the proposed desalination plant of Fortaleza, Brazil. *Desalination and Water Treatment*, 234:22–30, 2021. doi:[10.3389/fmars.2024.1377252](https://doi.org/10.3389/fmars.2024.1377252).

Raul Periáñez. A Lagrangian oil spill transport model for the Red Sea. *Ocean Engineering*, 217:107953, 2020. doi:[10.1016/j.oceaneng.2020.107953](https://doi.org/10.1016/j.oceaneng.2020.107953).

Pololu Robotics and Electronics. Pololu 3.3V step-up/step-down voltage regulator, 2025a. URL <https://www.pololu.com/product/2122>. Last visited: 08/12-2025.

Pololu Robotics and Electronics. Pololu 5V step-up/step-down voltage regulator, 2025b. URL <https://www.pololu.com/product/4082>. Last visited: 08/12-2025.

Jean Rabault, Graig Sutherland, Olav Gundersen, Atle Jensen, Aleksey Marchenko, and Øyvind Breivik. An open source, versatile, affordable waves in ice instrument for scientific measurements in the Polar Regions. *Cold Regions Science and Technology*, 170:102955, 2020. doi:[10.1016/j.coldregions.2019.102955](https://doi.org/10.1016/j.coldregions.2019.102955).

Jean Rabault, Takehiko Nose, Gaute Hope, Malte Müller, Øyvind Breivik, Joey Voermans, Lars Robert Hole, Patrik Bohlinder, Takuji Waseda, Tsubasa Kodaira, Tomotaka Katsuno, Mark Johnson, Graig Sutherland, Maiin Johansson, Kai Haakon Christensen, Adam Garbo, Atle Jensen, Olav Gundersen, Aleksey Marchenko, and Alexander Babanin. Openmetbuoy-v2021: An easy-to-build, affordable, customizable, open-source instrument for oceanographic measurements of drift and waves in sea ice and the open ocean. *Geosciences*, 12(3):110, 2022. doi:[10.3390/geosciences12030110](https://doi.org/10.3390/geosciences12030110).

Kaus Raghukumar, Grace Chang, Frank Spada, and Tim Jannsen. Directional spectrum measurements by the spotter: a new developed wave buoy, 2019. URL <https://scholarworks.uno.edu/oceanwaves/2019/Session2/1/>. Proc. Ocean Waves Workshop. Last visited: 08/12-2025.

Ian A. Raphael, Donald K. Perovich, Christopher M. Polashenski, and Robert L. Hawley. A low-cost, autonomous system for distributed snow depth measurements on sea ice. *EGU Sphere*, 2025:1–25, 2025. doi:[10.5194/tc-19-6059-2025](https://doi.org/10.5194/tc-19-6059-2025).

Giovanni Romagnoni, Kristina Øie Kvile, Knut-Frode Dagestad, Anne Maria Eikeset, Trond Kristiansen, Nils Chr. Stenseth, and Øystein Langangen. Influence of larval transport and temperature on recruitment dynamics of North Sea cod (*Gadus morhua*) across spatial scales of observation. *Fisheries Oceanography*, 29(4):324–339, 2020. doi:[10.1111/fog.12474](https://doi.org/10.1111/fog.12474).

Charalampos Nikolaos Roukounis and Vassilios A. Tsihrintzis. Indices of coastal vulnerability to climate change: a review. *Environmental Processes*, 9(2):29, 2022. doi:[10.1007/s40710-022-00577-9](https://doi.org/10.1007/s40710-022-00577-9).

Seeed Studio. LoRa wireless module - powered by STM32WLE5 datasheet, 2023. URL https://files.seeedstudio.com/products/317990687/res/LoRa-E5%20module%20datasheet_V1.1.pdf. Last visited: 08/12-2025.

Dallas Semiconductor. DS18B20 programmable resolution 1-wire digital thermometer, 2025. URL <http://cdn.sparkfun.com/datasheets/Sensors/Temp/DS18B20.pdf>. Last visited: 08/12-2025.

Andrew Olaf Shelton, Ana Ramón-Laca, Abigail Wells, Julia Clemons, Dezhang Chu, Blake E. Feist, Ryan P. Kelly, Sandra L. Parker-Stetter, Rebecca Thomas, Krista M. Nichols, and Linda Park. Environmental DNA provides quantitative estimates of Pacific hake abundance and distribution in the open ocean. *Proceedings of the Royal Society B*, 289(1971):20212613, 2022. doi:[10.1098/rspb.2021.2613](https://doi.org/10.1098/rspb.2021.2613).

Anne C. Sigleo, Calvin W. Mordy, Phyllis Stabeno, and Walter E. Frick. Nitrate variability along the oregon coast: Estuarine–coastal exchange. *Estuarine, Coastal and Shelf Science*, 64(2-3):211–222, 2005. doi:[10.1016/j.ecss.2005.02.018](https://doi.org/10.1016/j.ecss.2005.02.018).

SmartOcean, 2016. URL <https://www.smartocean-shop.com/>. Last visited: 08/12-2025.

Ryo Sugimoto, Akihide Kasai, Toshihiro Miyajima, and Kouichi Fujita. Transport of oceanic nitrate from the continental shelf to the coastal basin in relation to the path of the kuroshio. *Continental Shelf Research*, 29(14):1678–1688, 2009. doi:[10.1016/j.csr.2009.05.013](https://doi.org/10.1016/j.csr.2009.05.013).

Svein Sundby and Trond Kristiansen. The principles of buoyancy in marine fish eggs and their vertical distributions across the world oceans. *PloS one*, 10(10):e0138821, 2015. doi:[10.1371/journal.pone.0138821](https://doi.org/10.1371/journal.pone.0138821).

Jim Thomson, Phil Bush, Viviana Castillo Contreras, Nate Clemett, Jacob Davis, Alex de Clerk, Emily Iseley, Edwin James Rainville, Brenton Salmi, and Joe Talbert. Development and testing of microSWIFT expendable wave buoys. *Coastal Engineering Journal*, 66(1):168–180, 2024. doi:[10.1080/21664250.2023.2283325](https://doi.org/10.1080/21664250.2023.2283325).

Alexandra Toimil, Inigo J Losada, Paula Camus, and Pedro Díaz-Simal. Managing coastal erosion under climate change at the regional scale. *Coastal Engineering*, 128:106–122, 2017. doi:[10.1016/j.coastaleng.2017.08.004](https://doi.org/10.1016/j.coastaleng.2017.08.004).

Haiwen Tu, Xiaodi Wang, Lin Mu, and Kai Xia. Predicting drift characteristics of persons-in-the-water in the South China Sea. *Ocean Engineering*, 242:110134, 2021. doi:[10.1016/j.oceaneng.2021.110134](https://doi.org/10.1016/j.oceaneng.2021.110134).

Asaf Tzachor, Ofir Hendel, and Catherine E. Richards. Digital twins: a stepping stone to achieve ocean sustainability? *npj Ocean Sustainability*, 2(1):16, 2023. doi:[10.1038/s44183-023-00023-9](https://doi.org/10.1038/s44183-023-00023-9).

Lars Umlauf and Hans Burchard. Second-order turbulence closure models for geophysical boundary layers. a review of recent work. *Continental Shelf Research*, 25(7-8):795–827, 2005. doi:[10.1016/j.csr.2004.08.004](https://doi.org/10.1016/j.csr.2004.08.004).

Mangalore Vikas and G.S. Dwarakish. Coastal pollution: a review. *Aquatic Procedia*, 4:381–388, 2015. doi:[10.1016/j.aqpro.2015.02.051](https://doi.org/10.1016/j.aqpro.2015.02.051).

Jeremy P. Wilkinson, Pushkar M. Wadke, David Meldrum, D. Mercer, Martin Doble, and Peter Wadhams. The autonomous measurement of waves propagating across the Arctic Ocean. In *OCEANS 2007*, pages 1–7. IEEE, 2007. doi:[10.1109/OCEANS.2007.4449329](https://doi.org/10.1109/OCEANS.2007.4449329).

Julie E. Wood, Jacob Silverman, Barak Galanti, and Eli Biton. Modelling the distributions of desalination brines from multiple sources along the Mediterranean coast of Israel. *Water Research*, 173:115555, 2020. doi:[10.1016/j.watres.2020.115555](https://doi.org/10.1016/j.watres.2020.115555).

Daeun Yim, Jiwon Chung, Yulim Cho, Hyunji Song, Daehan Jin, Sojeong Kim, Sungwook Ko, Anthony Smith, and Austin Riegsecker. An experimental LoRa performance evaluation in tree farm. In *2018 IEEE sensors applications Symposium (SAS)*, pages 1–6. IEEE, 2018. doi:[10.1109/SAS.2018.8336764](https://doi.org/10.1109/SAS.2018.8336764).

Oliver Zielinski. The history and future of the secchi disk. *Angelo Secchi and Nineteenth Century Science: The Multidisciplinary Contributions of a Pioneer and Innovator*, pages 215–224, 2021. doi:[10.1007/978-3-030-58384-2_13](https://doi.org/10.1007/978-3-030-58384-2_13).

Appendix A: Open-Source Release

All firmware for the buoy, base station and digital platform will be made available at <https://github.com/larswd/OpenLoraBuoy> after publication in the peer-reviewed literature at the latest. This repository also contain the printed circuit board (PCB) designs for the buoy and base station, alongside a maintained component list with links to a distributor.